Shock Waves (1994) 4:119–125

Shock Waves

The application of coherent anti-Stokes Raman scattering to temperature measurements in a pulsed high enthalpy supersonic flow

D.R.N. Pulford[1], D.S. Newman[2], A.F.P. Houwing[1], R.J. Sandeman[1]

[1] Physics Department, Science Faculty, Australian National University, Canberra A.C.T. 0200, Australia
[2] Department of Applied Physics, University of Central Queensland, Rockhampton, QLD 4702, Australia

Received May 26, 1994; accepted August 6, 1994

Abstract. Broadband single pulse coherent anti-Stokes Raman scattering (CARS) experiments employing a folded box phase matching geometry in a shock tunnel flow are presented. Rovibrational spectra of molecular nitrogen, produced at the exit of a pulsed supersonic nozzle for a range of flow enthalpies, are examined. Difficulties peculiar to the application of the optical technique to a high enthalpy pulsed flow facility are discussed and measurements of flow temperatures are presented. Theoretically calculated values for temperatures based upon algorithms used to determine shock tunnel flow conditions agree well with experimental measurements using the CARS technique.

Key words: Coherent Anti-Stokes Raman Scattering, Shock Tunnel, Thermometry

1. Introduction

Coherent Anti-Stokes Raman Scattering (CARS) has become a proven diagnostic technique over the past decade for probing processes occuring in hostile environments (Knapp and Hindelang 1981; Bruckner and Hindelang 1983). It is a non-intrusive, species specific technique whose high temporal and spatial resolution can be exploited to great advantage in shock tunnel experiments. It is a coherent process in which the final signal emerges as a well defined beam resulting in a high detection efficiency and rejection of spurious interfering effects. This is particularly important in applications to shock tunnel flows, where high intensity isotropic background radiation is caused by the presence of metallic impurities, such as nickel, chromium and iron. These impurities appear to be introduced into the flow as a result of erosion of the shock tube walls in the nozzle reservoir region, which is exposed to extremely high temperatures and pressures. The concentration of some of these impurities have been measured using hook interferometry (Ebrahim and Sandeman 1977), which has shown that the levels can be as high as 300 ppm. The presence of this background radiation presents a problem for other optical diagnostic techniques such as laser induced fluorescence (LIF) because of the isotropic nature of the LIF signal. The CARS signal, however, has an extremely low divergence and can be separated relatively easily from the background radiation through the use of a spatial mask. The LIF technique has been used successfully in a large range of applications, including shock tube (Palmer et al. 1991) and tunnel (Palmer et al. 1992) flows. However, in these cases the flow enthalpies have been much smaller than those considered in the current paper.

Because the CARS process is a nonlinear optical phenomenon, there is a requirement for high laser intensities to produce strong signals. This requirement necessitates the focussing of laser beams to a very small interaction volume. Consequently, the technique is restricted to point wise measurements and a large amount of data is required to determine spatial variations of the measured quantities throughout the flow being studied. In a pulsed flow facility, this either places a very stringent requirement on shot-to-shot repeatability, or necessitates the accumulation of even more data to allow statistical averaging. Linear optical methods such as LIF, on the other hand, allows one to produce two dimensional maps with a single pulse, and is thus much more efficient as far as data accumulation rates are concerned. LIF has been shown to be an extremely useful technique applicable to the measurement of gaseous chemical species concentrations (Stepowski and Cottereau 1981; Dyer and Crosley 1982; Hanson 1987; Hanson et al. 1990) rotational and vibrational temperatures (Chan and Daly 1980a; Lee et al. 1987) and flow velocities (Hiller and Hanson 1988) in a range of environments, including atmospheric flames, internal combustion engines, nozzle flows and shock wave studies. However, to enable accurate measurements of these parameters from the LIF signals, one must use appropriate rate models that account for excitation dynamics (Chan and Daly 1980b), redistribution of rotational (Berg and Shackleford 1979) and vibrational levels (Campbell 1982), saturation (Seitzmann and Hanson 1991; Lucht et al. 1990; Carter et al. 1987; Lucht et al. 1982) and depletion (Campbell 1984) effects and collisional quenching (Barlow and

Correspondence to: A.F.P. Houwing

Colligan 1991). Collisional quenching is a very important consideration in the application of LIF to pulsed high enthalpy flows because of the high collision rates in such environments. Variations of the LIF method, for example laser induced predissociation fluorescence (LIPF) (Andresen et al. 1988), enable one to produce fluorescence signals which are unaffected by collisional deexcitation, however, the signals thus produced are much weaker, so it can be difficult to separate the LIPF signals from the high intensity background. The CARS technique does not suffer from the aforementioned disadvantages, although at some conditions saturation (Lucht and Farrow 1988; 1989) effects become important. In principle, both species concentration and temperature can be determined from the CARS signal. Species concentration is related to the intensities of the spectral features while temperature can be inferred from the distribution of molecular rotational and vibrational states observed in the CARS spectrum. The simultaneous determination of these properties is extremely useful in shock tunnel research where situations of chemical and thermal non-equilibrium can be routinely encountered.

The CARS technique has been applied to the measurement of gaseous chemical species concentrations (Eckbreth, Anderson 1985, 1987; Lucht 1987) and temperatures (Knapp and Hindelang 1981; Brückner and Hindelang 1983; Eckbreth et al. 1984) in a range of combustion and shock tube environments. Previous applications of CARS to measure temperatures behind shock waves were performed in a shock tube configuration (rather than a shock tunnel) using collinear CARS (Knapp and Hindelang 1981; Brückner and Hindelang 1983) where spatial resolution was limited to the dimensions of the confocal parameters of the laser beams. The conditions examined in this earlier work were in the stagnation region behind the reflected shock wave, where densities were higher and test times much longer than those being considered in the present work. The motivation for applying single shot CARS to a high enthalpy pulsed flow is based on future experimental work designed to measure the fuel-air mixing and combustion rates in a supersonic combustion engine (SCRAMJET) (Stalker and Morgan 1984; Stalker et al. 1988) at high flow enthalpies. In this proposed work, the stagnation enthalpy will range from 4 to 12 MJ/kg and the temperature from 1000 to 3000 K. These values are significantly higher than those corresponding to the conditions of previous supersonic combustion CARS experiments (Anderson and Eckbreth 1992), which were performed in a flow facility having a runtime between 60 and 90 s. By comparison, the steady flow period of our pulsed facility is of the order of 500 μs. Hence, whereas averaging techniques could be used in the longer running facility, single shot measurements must be made in the pulsed facility. This fact leads to a number of difficulties, which will be discussed in more detail below.

2. Theoretical considerations

2.1. Coherent anti-Stokes Raman scattering

The theoretical description of CARS is now well established and has been described in several recent reviews (Eckbreth 1988; Clark, Hester 1988). Figure 1 illustrates the basic features required for the production of the CARS spectrum. Briefly, for two colour CARS, incident laser beams at frequencies ω_1 and ω_2, commonly referred to as the pump and Stokes beams respectively, interact through the third order non-linear susceptibility $\chi^{(3)}(\omega_3)$ of the medium to generate a polarization field which acts as a source for anti-Stokes radiation at frequency $\omega_3 = 2\omega_1 - \omega_2$. For plane waves, the intensity $I_3(\omega_3)$ of the CARS beam can be expressed as

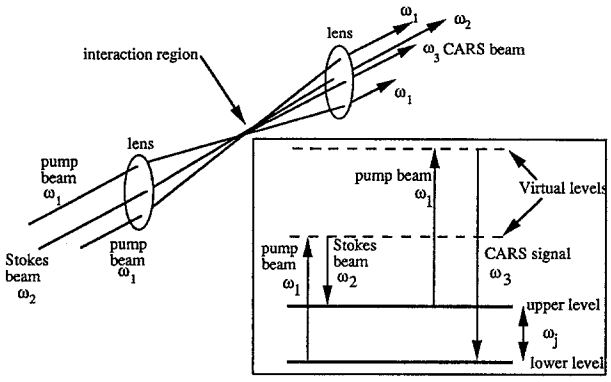

Fig. 1. Basic optical configuration for production of a CARS signal (the relevant energy level diagram is illustrated at the bottom right of the figure)

$$I_3(\omega_3) = \left(\frac{4\pi\omega_3}{c^2 n_3}\right)^2 I_1^2(\omega_1) I_2(\omega_2) \times |3\chi^{(3)}(\omega_3)|^2 \ell^2 \mathrm{sinc}^2(|\Delta\mathbf{k}|\ell) \ldots \quad (1)$$

where ℓ is the interaction length, $\Delta\mathbf{k}$ is the phase mismatch of the CARS beam and pump and probe beams, c is the velocity of light and n_3 is the refractive index at ω_3. The phase mismatch is given by

$$\Delta\mathbf{k} = \mathbf{k}_3 + \mathbf{k}_2 - 2\mathbf{k}_1 \ldots \quad (2)$$

where $\mathbf{k}_1$, $\mathbf{k}_2$ and $\mathbf{k}_3$ are the wave vectors of the pump, Stokes and CARS beams, respectively. The nonlinear susceptibility can be written in terms of a resonant and nonresonant part χ^{nr},

$$\chi^{(3)} = \sum_j (\chi' + i\chi'')_j + \chi^{\mathrm{nr}} \ldots \quad (3)$$

where $i = \sqrt{-1}$; χ' and χ'' are the real and imaginary components, respectively, of the resonant part; and χ^{nr} is the contribution from electrons and remote resonances. The resonant susceptibility associated with a homogoneously broadened Raman transition j is

$$(\chi' + i\chi'')_j = \frac{4\pi c^4}{h\omega_2^4} N \Delta_j g_j \left(\frac{\partial\sigma}{\partial\Omega}\right)_j \times \frac{\omega_j}{\omega_j^2 - (\omega_1 - \omega_2)^2 - i\Gamma_j(\omega_1 - \omega_2)} \ldots \quad (4)$$

where h is Planck's constant; N the total species number density; Δ_j the population difference between the levels involved in the transition; g_j the line strength factor; $(\partial\sigma/\partial\Omega)_j$ the Raman cross section, Γ_j the Raman linewidth; and ω_j the transition frequency.

2.2. *Determining flow temperatures and species concentrations*

From equation (1), we note that the experimental measurement of I_3 for an isolated Raman transition allows one to determine $\chi^{(3)}$. Provided the nonresonant component is small (or can be accounted for) and relevant spectroscopic data is available, the measurement of the susceptibility allows the determination of $N\Delta_j$ from (3) and (4). If one assumes a Boltzmann distribution based on the rotational (T_r) and vibrational (T_v) temperatures for Δ_j and a sufficient number of isolated lines are studied, it is possible to determine T_r and T_v using data fitting techniques. The determination of N requires knowing the values of $I_1(\omega_1)$, $I_2(\omega_2)$, ℓ and $\Delta\mathbf{k}$. Alternatively, one can determine the value of N through a calibration technique, which compares I_3 to the signal I_3' produced in a reference cell containing a known density N'. By using an appropriately placed beamsplitter, it is possible to preserve the values of ℓ and $\Delta\mathbf{k}$ and to fix the ratios I_1'/I_1 and I_2'/I_2, where I_1' and I_2' are the intensities of the pump and Stokes beams in the reference cell. Since the temperature T' in the reference cell is known, the value of the population difference Δ_j' can also be determined there. The value of Δ_j in the test section is determined through the data fitting techniques used to determine T_r and T_v. Hence there is sufficient information to determine N from the ratio I_3/I_3'. It is important to note that the above discussion implicitly assumes that the wave fronts of the pump and Stokes beams are plane. In reality though, the wave fronts are near-Gaussian and are strictly only plane at the position of the beam waists. A study of the effects of Gaussian beam focusing has shown (Bjorklund 1975) that the dependence of the CARS signal on ℓ and $\Delta\mathbf{k}$ given in equation (1) is only correct if the beam waists lie well outside the medium. Furthermore, for a near-Gaussian wave front, $\Delta\mathbf{k}$ will not be strictly constant throughout the interaction region. The best way to take these complicating effects into account is to replace the quantity $\ell^2\,\mathrm{sinc}^2(|\Delta\mathbf{k}|\ell)$ by some undetermined function $f(\ell, \mathbf{k}_1, \mathbf{k}_2, \mathbf{k}_3)$, which can be factored out in the calibration process described above.

For broadband CARS, ω_2 has a range of values; the Stokes laser intensity I_2 has a nonuniform intensity over this range; and the CARS signal I_3 is dispersed using a spectrometer. In this case, $I_3(\omega_3)$, as measured by a detector attached to the spectrometer, is a convolution of the pump laser profile, the Stokes laser profile, the Raman line profile and the instrument function of the spectrometer-detector system. Provided these convolutions are appropriately accounted for, the values of N, T_r and T_v can still be determined using data fitting and calibration techniques.

3. The experimental arrangement

In the measurements reported here, the folded box phase matching configuration was employed. In this configuration, the laser beams cross at a point, restricting the dimensions of the interaction volume and resulting in very high spatial resolution. The flow being investigated was the intake flow inside a supersonic combustion ramjet (SCRAMJET) engine at the exit of a nozzle of a free piston shock tunnel. The flow produced by this nozzle corresponds to the upstream conditions of the intake of the SCRAMJET engine studied in previous work (Stalker and Morgan 1984; Stalker et al. 1988). The objectives of the experiment were to measure the temperature and nitrogen species density of the supersonic stream inside the intake.

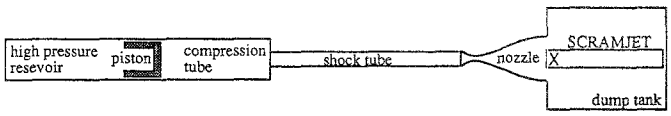

Fig. 2. Schematic of free piston shock tunnel. X indicates CARS interaction region

3.1. *The shock tunnel facility*

The present experiments were performed on the Australian National University's T3 free piston shock tunnel (Stalker 1972) (see Fig. 2) which produces variable high enthalpy flows as described briefly in the following. A high pressure reservoir containing air is set up behind a piston. In front of the piston in the compression tube is a relatively low pressure region containing a driver gas mixture of helium and argon. The compression tube and shock tube are separated by a metal diaphragm, having a predetermined rupture pressure. The shock tube is filled with the test gas (air in this case). At the end of the shock tube, is placed a converging diverging nozzle, whose exit is situated in a large dump tank. The shock tube and nozzle are separated by a very thin mylar diaphragm and the dump tank is evacuated to a very low pressure (less than 1 Pa) before each run. During an experimental run, the piston is released, compressing the helium and argon to very high pressure until the diaphragm bursts. When the diaphragm bursts a shock wave travels into the shock tube with a velocity that can be varied from 2 to 7 km/sec, by an appropriate choice of operating conditions. This shock wave (termed the primary shock) is followed by a contact surface, which separates the driver and test gases. When the shock wave reaches the end of the shock tube it is reflected and the thin mylar diaphragm covering the narrow entrance to the nozzle ruptures. The reflected shock wave interacts with the contact surface, which either accelerates or attenuates the shock depending on the acoustic impedance change across the contact surface. This interaction causes compression or expansion waves to modify the conditions behind the reflected shock in a nearly isentropic manner. Following the interaction process, the conditions in the nozzle reservoir region at the end of the shock tube become reasonably steady, resulting in steady flow through the nozzle and at its exit.

The conditions of the flow in the test section were selected by appropriate choices for: the partial pressures of argon and helium in the driver gas; the diaphragm rupture pressure; and the shock tube fill pressure. The pressures and transit times of the primary shock wave were measured with a number of piezoelectric transducers placed along the length of the shock tube. The last transducer also monitored the nozzle reservoir pressure. The flow conditions in the shock tube and the nozzle were calculated using an algo-

Table 1. Theoretically calculated shock tunnel flow conditions[a]

Condition	Stagnation Enthalpy (MJ/kg)	Temperature (K)	Pressure (kPa)
(I)	4.3 ± 0.1	1160 ± 70	99 ± 5
(II)	8.7 ± 0.3	2370 ± 140	124 ± 7
(III)	12.1 ± 0.4	3040 ± 180	114 ± 6

[a] Errors estimated from results given in Stalker and Morgan (1984)

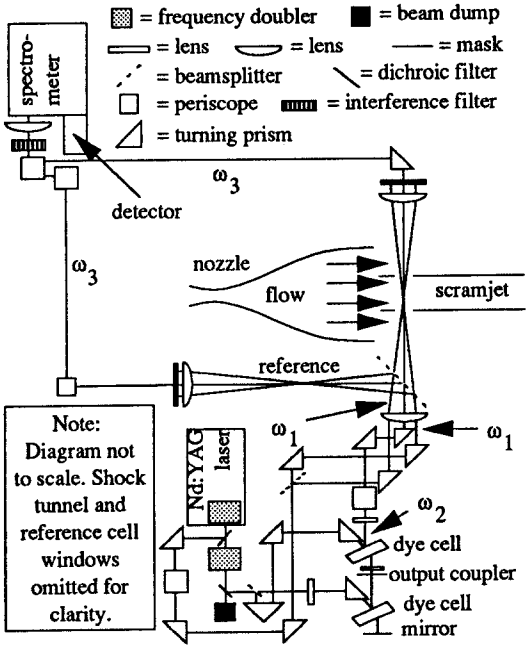

Fig. 3. The optical arrangement for CARS measurements in a pulsed flow

rithm developed by Vardavas (1984), based on the following assumptions. Thermodynamic equilibrium was assumed in the calculation of conditions after the primary shock, the reflected shock and following the interaction between the reflected shock and contact surface. In addition, this interaction was assumed to be isentropic. For the flow through the nozzle, a chemical reaction rate model was used. Thermal equilibrium was assumed throughout with $T_r = T_v$. Input data necessary for the calculations were: thermodynamic data of the test gas; the shock tube fill pressure; primary shock wave velocity; the nozzle reservoir pressure; and the nozzle geometry. The wall boundary layers and weak shock waves inside the intake duct of the SCRAMJET perturb the supersonic nozzle jet as it enters the intake. Hence conditions inside the intake will differ from those at the nozzle exit. However, the measurement of static pressure inside the duct indicates that the perturbation to the incoming flow is quite small. For this reason, it is assumed, in the current investigation, that the conditions inside the intake are identical to those at the nozzle exit. The test conditions calculated in this manner and used in the current experiments are summarised in Table 1. These conditions are very similar to those used in previous SCRAMJET studies (Stalker, Morgan 1984; Stalker et al. 1988).

3.2. Optical setup

The optical arrangement is illustrated in Fig. 3. The CARS system was based around a frequency doubled Nd:YAG laser (Quanta Ray GCR-4) giving approximately 1 J per pulse at 1064 nm with a typical pulse width of 8.5 ns. Frequency doubling produced a beam of 180 mJ at 532 nm (0.06 nm FWHM). At most, about 30% of the 1064 nm infra-red beam was converted to visible radiation by the frequency-doubling crystal. Following separation of the visible and infra-red beams by a dichroic beam splitter, the residual fundamental was passed through another frequency-doubler. The output from this second frequency-doubler was again separated into its wavelength components, with the residual infra-red beam being blocked by a beam-dump. The visible beam at 532 nm produced by the second frequency-doubler was used to pump a broadband dye laser which produced a 42 mJ beam at 607 nm (6.4 nm FWHM). This beam becaue the Stokes beam of the CARS process. The visible output from the first frequency-doubler was further divided into two beams, which became the pump beams of the CARS process. The Stokes and pump beams were then combined for folded box phase matching with a 500 mm focal length lens. At this lens the pump beams were separated by 25 mm giving a spatial interaction region approximately 2 mm in length and 200 μm in diameter. A 50% reflecting beamsplitter before the main focusing lens generated two interaction regions, one in the test section of the shock tunnel, the other in a calibration cell containing air at atmospheric pressure. Care was taken to ensure that both interaction regions had the same confocal parameters so that the reference signal from the calibration cell could be used to normalise the laser beam characteristics for the particular shot. The CARS signals generated were passed into a one meter spectrometer with a diffraction grating of 1800 lines/mm and imaged onto a gated dual microchannel plate image intensifier, fibre optically coupled to a charge injection device (CID) camera. The overall gain was about 10^6 and the final camera resolution 0.0097 nm/pixel. The chip was cooled by a Peltier device to 258 K to reduce thermal noise.

3.3. Timing procedures

An IBM compatible PC was employed to control the operation of the laser and camera systems and synchronize their triggering with the establishment of steady flow in the test section. The operation of the shock tunnel was monitored through a recoil motion transducer situated on the compression tube and three pressure transducers mounted along the shock tube. Before the shock tunnel was fired, the laser was operated at 10 Hz repetition rate for approximately 10 minutes while slowly increasing the output to full power to ensure that the laser and harmonic generating crystals could reach thermal equilibrium. On firing the shock tunnel the recoil of the compression tube activated the motion transducer whose signal was used to halt the repetitive firing mode of the laser and initialise it for a single shot. The shock wave travelling down the shock tube triggered a pressure transducer in the nozzle reservoir region which activated counter based delay circuits to trigger the

laser flashlamps, Q-switch and camera to capture an image when equilibrium flow conditions were established over the model. Typical delay times were of the order of 200–400 μs between the signal from this transducer and the firing of the flashlamps, dependent on shot enthalpy, and a fixed delay of 280 μs between flashlamps and Q-switch. The camera was triggered simultaneously with the Q-switch to provide a 90 ns detection window around the laser pulse.

4. Results

A series of CARS spectra of molecular nitrogen in the SCRAMJET were recorded for three conditions (here termed I, II and III) which are summarised in Table 1. A significant amount of processing of the raw data is required to account for: the profile of the Stokes laser; fluctuations in laser intensities; background noise; and convolution of the CARS signal with the instrument function. The experimental data were divided by a Gaussian fit to the dye laser spectrum to take into account its finite bandwith, while Fourier transform analysis was used to remove the high frequency structure. The processed spectra for the three conditions are presented as bold lines in Fig. 4, together with the theoretically determined spectra, which are presented as thin lines. A spectrum obtained from the calibration cell is presented in Fig. 4a, while spectra obtained from the flow are presented in Fig. 4b–d. The high frequency noise superimposed on the experimental spectra is due to intensity fluctuations in the spectrum of the dye laser. The peaks in the experimental spectra represent rotationally averaged vibrational states of the molecular nitrogen ground electronic state $X^1\sum_g$. The vibrational transitions observed were: $(v', v'') = (1, 0)$ for all three flow conditions; and $(v', v'') = (2, 1)$ and $(v', v'') = (3, 2)$ for conditions II and III:

In order to determine the rotational and vibrational temperatures, corresponding to the different CARS spectra, the following method was used. Theoretical CARS spectra were generated from the isolated line model (Hall 1979) assuming that rotational and vibrational equilibrium was established (i.e. $T_r = T_v$). The use of the isolated line model was expected to be a reasonable approximation because the pressure in the test section was typically of the order of 100 kPa during the experiment. These spectra were convoluted with the pump laser linewidth (assumed to be 0.02 nm) and an instrument function due to the detector. The instrument function accounted for the spectrometer dispersion, distortion introduced by the image intensifier and the pixel dimensions on the CID chip. This was estimated from measurements of the FWHM of the 632.82 nm HeNe line and assumed to be a triangular function with 0.056 nm FWHM. This data was then compared, using a least squares fitting procedure, to theoretical spectra calculated over the temperature range 250–3100 K in 25 K intervals. The best fitting theoretical spectra obtained in this way are represented by the thin lines in Fig. 4. The temperatures obtained from the mean of three shots at each of the three enthalpy conditions in the shock tunnel are presented in Table 2 along with theoretical values of flow temperatures in the SCRAMJET intake. The theoretical values were determined as described in Sect. 3.1.

Table 2. Comparison between calculated and measured free stream temperatures

Condition	Theoretical temperature[a]	Experimental temperature
(I)	1160 ± 70	1140 ± 130
(II)	2370 ± 140	2642 ± 120
(III)	3040 ± 180	2917 ± 120

[a] Errors estimated from results given in Stalker and Morgan (1984)

The experimental and theoretical temperatures are in good agreement to within experimental error. Further justification for the validity of the experimental method and data analysis can be gained from the calibration cell spectra which yielded a room temperature of 300 K.

Due to the single shot nature of the experiment, shot to shot variability of the flow conditions is believed to be contributing to the largest errors to temperature determination with other random sources of noise from intensity fluctuations in the dye and pump laser beams. The camera also contributes a systematic error due to a nonlinear noise background from self-heating in the CID chip which varies its dynamic range across its active surface. When these effects are taken into consideration, the errors in temperature determination on a single shot basis are estimated to be ± 120 K. The errors quoted in Table 2 represent the single shot error and statistical error from combination of the individual measurements.

Attempts to produce accurate number density measurements were unsuccessful due to difficulties experienced with matching the confocal parameters in the calibration cell to those in the flow. An investigation into the possible causes for these difficulties identified that mechanical stresses in the shock tunnel window mountings are responsible for movement in the windows, which partially destroys the overlap of the pump and Stokes beam in the test section. This problem is overcome in current work through prestressing the window mounts prior to the alignment of the CARS system and by using compensating plates in the optical arrangement.

5. Discussion and conclusions

As mentioned in the introduction, CARS signals can be affected by saturation effects (Lucht, Farrow 1988, 1989). These tend to cause an overestimation of the flow temperature by stimulated Raman pumping into higher vibrational levels, and are important considersations at high laser powers. One way to ascertain whether these effects are occurring is to compare CARS spectra generated with high pump and Stokes laser powers to the spectra generated with lower laser powers. If the appropriately normalised CARS signals are not dependent upon laser powers, saturation effects can be neglected. This is an important consideration because high laser powers are necessary in the high enthalpy environment generated in a shock tunnel to ensure that the signal levels are significantly larger than the background radiation. Furthermore, high laser powers are required at high temperatures and low densities (where the quantity $N\Delta_j$ can become very small) to ensure detectable signal levels. In the current work, the pump and Stokes laser powers were each

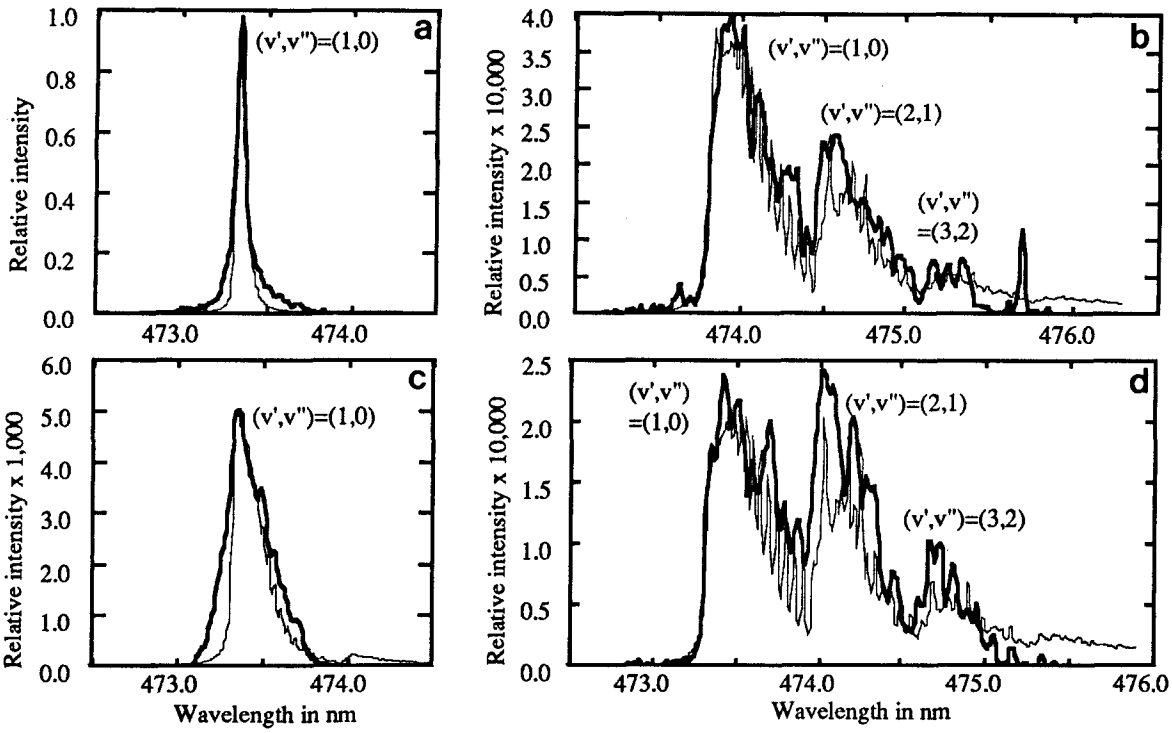

Fig. 4a–d. The thin line indicates theoretical CARS spectra and the thick line experimental results. **a** Calibration cell spectra, **b** flow condition I, **c** flow condition II, **d** flow condition III

varied by a factor of ten without variation in the spectral profile of the signal produced in either the reference cell or signals produced in the test region for a no flow condition. It was not possible to vary the laser powers for a flow condition because varying the power of the beams significantly meant that a reasonable signal level could not be obtained.

The spectra in Fig. 4 are single shot spectra and show a great deal of noise which is believed to have been produced by mode noise in the Stokes laser. This noise produces fluctuations from shot to shot in the spectral profile. Steps are being taken to reduce this effect by measuring the Stokes laser profile with each shot and dividing single shot CARS spectra by the corresponding Stokes laser spectral profile. In addition, noise is produced on the camera by thermal electrons produced in the camera. The camera is currently cooled to 256 K and the production of the thermal electrons is still present. Cooling down the camera further may damage the chips used in the camera, so further cooling has not been implemented. If one compares the numerically predicted values of the flow temperatures with the experimentaly measured values, it is found that the computer code agrees within experimental error. Furthermore, based on the following arguments, the assumption of thermal equilibrium in the free stream flow appears to be reasonable. From energy considerations, a departure from thermal equilibrium ($T_v \neq T_r$) would be apparent through a deviation of the theoretical and experimentally measured CARS spectra. Since in the fitting techniques used here it was assumed that $T = T_v = T_r$ this deviation would have been observed as a larger value for T. The close agreement between the theoretical and experimental values for T suggests that thermal equilibrium exists in the flow conditions studied.

Acknowledgement. We express our thanks to Mr. Paul Walsh for his competent operation of the shock tube and anciliary equipment, and to Mr. Graeme Pike and Mr. Paul Tant for their excellent craftmanship in the construction of the scramjet model. We are grateful to Dr. Richard Morgan for his design of the scramjet model. This work has been financially supported by the Australian Research Council, the Sir Ross and Sir Keith Smith Fund, and NASA contract number NAGW 1467.

References

Anderson TJ, Ecbreth AC (1992) Simultaneous coherent anti-Stokes Raman spectroscopy measurements in hydrogen-fueled supersonic combustor. J Propulsion 8: 7

Andresen P, Bath A, Gröger W, Lülf HW, Meijer G, ter Meulen JJ (1988) Laser-induced fluorescence with tunable excimer lasers as a possible method for instantaneous temperature field measurements at high pressures: checks with an atmospheric flame. Appl Opt 27: 365

Barlow RS, Colligan A (1991) Linear LIF measurements of OH in nonpremixed methane-air flames: When are quenching corrections unnecessary? AIAA 29th Aerospace Sciences Meeting, Reno: AIAA 91-0179

Berg JO, Shackleford WL (1979) Rotational redistribution effect on saturated laser-induced fluorescence. Appl Opt 18: 2093

Bjorklund GC (1975) Effects of focussing on 3rd-order nonlinear processes in isotropic media. IEEE J Quant Electron 11: 287

Brückner S, Hindelang FJ (1983) Methods for improving the performance of CARS measurements in shock tubes. Proceedings of the 14th International Symposium on Shocktubes and Shock Waves, University of Sydney, pp 615–620

Campbell DH (1982) Vibrational level relaxation effects on laser-induced fluorescence measurements of hydroxide number density in a methane-air flame. Appl Opt 21: 2912

Campbell DH (1984) Collisional effects on laser-induced fluorescence measurements of hydroxide concentrations in a combustion environment: Effects for $v' = 0$ excitation. Appl Opt 23: 689

Carter CD, Salmon JT, King GB, Laurendeau NM (1987) Feasibility of hydroxyl concentration measurements by laser-saturated fluorescence in high-pressure flames. Appl Opt 26: 4551

Chan C, Daily JW (1980a) Measurement of temperature in flames using laser induced fluorescence spectroscopy of OH. Appl Opt 19: 1963

Chan C, Daily JW (1980b) Laser excitation dynamics of OH in flames. Appl Opt 19: 1357

Clark RJH, Hester RE (1988) In: Advances in Non-Linear Spectroscopy (Advances in Spectroscopy, Vol 15), John Wiley and Sons Ltd, pp 193–237

Dyer MJ, Crosley DR (1982) Two-dimensional imaging of OH laser-induced fluorescence in a flame. Opt Lett 7: 382

Ebrahim N, Sandeman RJ (1977) Spatially resolved excitation temperature measurements in a hypersonic flow using the hook method. Appl Opt 16: 1376

Eckbreth AC (1988) In: Laser Diagnostics for Combustion Temperature and Species. Abacus Press (now Gordon and Breach), Kent, England, UK, pp 3–24

Eckbreth AC, Anderson TJ (1985) Dual broadband CARS for simultaneous multiple species measurements. Appl Opt 24: 2325

Eckbreth AC, Anderson TJ (1987) Multi-color CARS for simultaneous measurements of multiple species. Society of Photo-Optical Instrumentation Engineers 742: 34

Eckbreth AC, Dobbs GM, Stufflebeam JH, Tellex PA (1984) CARS temperature and species measurements in augmented jet engine exhausts. Appl Opt 23: 1328

Hall RJ (1979) CARS spectra of combustion gases. Combustion and Flame 35: 47

Hanson RK (1987) Combustion diagnostics: Planar flowfield imaging. Twenty-First International Symposium on Combustion. The Combustion Institute Pittsburgh PA, pp 1677–1691

Hanson RK, Seitzman JM, Paul PH (1990) Planar laser-fluorescence imaging of combustion gases. Appl Phys B 50: 441

Hiller B, Hanson RK (1988) Simultaneous planar measurements of velocity and pressure fields in gas flows using laser-induced fluorescence. Appl Opt 27: 33

Knapp K, Hindelang FJ (1981) Measurement of temperatures in a shock tube by coherent anti-Stokes Raman spectroscopy (CARS). Proceedings of the 13th International Sympsoium on Shocktubes and Shock Waves, Niagara Falls, pp 132–137

Lee MP, Paul PH, Hanson RK (1987) Quantitative imaging of temperature fields in air using planar laser-induced fluorescence of O_2. Opt Lett 12: 75

Lucht RP (1987) Three laser CARS measurements of two species. Optics Lett 12: 78

Lucht RP, Farrow RL (1988) Calculation of saturation line shapes and intensities in coherent anti-Stokes Raman scattering spectra of nitrogen. Journal of the Optical Society of America B 5: 1243

Lucht RP, Farrow RL (1989) Saturation effects in coherent anti-Stokes Raman scattering spectroscopy of hydrogen. Journal of the Optical Society of America B 6: 2313

Lucht RP, Laurendeau NM, Sweeney DW (1982) Temperature measurements by two-line laser-saturated OH fluorescence in flames. Appl Opt 21: 3729

Lucht RP, Sweeney DW, Laurendeau NM (1980) Balanced cross-rate model for saturated molecular fluorescence in flames using a nanosecond pulse length laser. Applied Optics 19: 3295

Palmer JL, McMillin BK, Hanson RK (1992) Planar laser-induced fluorescence imaging of velocity and temperature in shock tunnel free jet flow. 30th Aerospace Sciences Meeting and Exhibit, Reno, NV, January 6–9

Palmer JL, McMillin BK, Lee MP, Hanson RK (1991) Two-dimensional imaging of shock tube flows using planar laser-induced fluorescence. 18th International Symposium of Shock Waves, Sendai, Japan

Seitzman JM, Hanson RK (1991) Quantitative fluorescence imaging: A comparison of linear, predissociative and saturated pumping techniques. American Institute of Aeronautics and Astronautics, 30th Aerospace Sciences Meeting, Reno, NV, paper 92-0879

Stalker RJ (1972) Development of a hypervelocity wind tunnel. Aero J of R Aero Soc 76: 374

Stalker RJ, Morgan RG (1984) Supersonic hydrogen combustion with a short thrust nozzle. Combustion and Flame 57: 55

Stalker RJ, Morgan RG, Netterfield MP (1988) Wave processes in scramjet thrust generation. Combustion and Flame 77: 63

Stepowski D, Cottereau MJ (1981) Study of the collisional lifetime of hydroxyl ($^2\Sigma^+, v' = 0$) radicals in flames by time-resolved laser-induced fluorescence. Combust Flame 40: 65

Vardavas IM (1984) Modelling reactive gas flows within shock tunnels. Aust J Phys 37: 157